Additional features in HAMS-MREL
a new open-source BIEM solver for offshore energy applications

Raghavan, Vaibhav; Metrikine, Andrei; Lavidas, George

DOI
10.36688/ewtec-2025-700

Publication date
2025

Document Version
Final published version

Published in
Proceedings of the European Wave and Tidal Energy Conference

Additional features in HAMS-MREL: a new open-source BIEM solver for offshore energy applications

V. Raghavan, A.V. Metrikine, and G.Lavidas

Abstract—**HAMS-MREL is a recently developed open-source BIEM (Boundary Integral Equation Method) solver, which allows for the solution of the diffraction and radiation problem for multiple floating rigid structures, taking into account their interaction. This solver has shown to be highly accurate when compared with semi-analytical solutions/commercial solver WAMIT, within a computationally efficient framework that is parallelized. The solver is currently capable of providing the hydrodynamic coefficients (added mass and radiation damping) and exciting forces for all 6 rigid body modes per body. With this research, the solver has been extended significantly to include the following features for the multiple body interaction problem 1) Removal of irregular frequencies, 2) Global symmetry, 3) Wave fields and 4) Generalized modes. This study contributes further to the open-source domain with the development of highly accurate numerical tools for the accelerated deployment of offshore renewables.**

Index Terms—**HAMS-MREL, BIEM, Wave fields, Irregular frequencies, Symmetry, Generalized modes**

I. Introduction

Tools and simulations based on frequency domain calculations have been extensively used in the field of offshore renewables for analysing arrays, due to their numerous benefits: (a) they can provide accurate and reliable results at the preliminary design stage, (b) their output (frequency-dependent hydrodynamic quantities) are often required for their integrated analysis in the time domain, and (c) they have a significantly lower computational requirement as compared to higher fidelity models such as Computational Fluid Dynamics (CFD) ([1], [2]). Among these methods, BIEM based on linear potential flow theory has been one of the most popular choices.

There are many commercial BIEM solvers with WAMIT [3], WADAM [4], Hydrostar [5] and ANSYS AQWA [6] being some of the most popular. Then there are in-house solvers, such as DIFFRACT [7] and OREGEN-BEM [8] that are neither commercial nor open-source. These have been extensively developed and utilized for multiple body BIEM calculations with Wave Energy Converters (WEC) and WEC arrays ([8]–[13]).

V. R., A. M. and G. L. are part of the Offshore Engineering Section of the Delft University of Technology (TU Delft), Stevinweg 1, 2628 CN Delft, The Netherlands (e-mail: v.raghavan@tudelft.nl, a.metrikine@tudelft.nl, g.lavidas@tudelft.nl).

Digital Object Identifier:
https://doi.org/10.36688/ewtec-2025-700

A lot of work has also been put into the development of open source alternatives. When considering the open-source domain for array calculations (multiple body simulations), there are BIEM codes such as Nemoh 2.x [14] , Nemoh 3.0 [15] and Capytaine [16] which are being widely used by the renewable energy community. All these solvers can calculate the diffraction and radiation solutions for multiple body wave-structure interaction problems, providing the hydrodynamic coefficients, excitation forces, free surface elevations and pressure fields.

HAMS-MREL (Marine Renewable Energies Lab) is a recently developed BIEM solver from Raghavan et.al. [17], that has added to the open-source domain. It is based on the single body open-source BIEM solver HAMS [18]. HAMS has been validated with analytical, semi-analytical, commercial solvers and experiments for a number of different structural geometries in the field of renewable energy ([18]–[23]). HAMS is also computationally much faster than other open-source BIEM solvers such as Nemoh 2.x and Capytaine ([23], [24]).

HAMS-MREL builds upon the framework of single body solver HAMS, to solve the multiple body fluid-structure interaction problem for the diffraction radiation problem using mixed source/dipole boundary integral equations, to produce the hydrodynamic coefficients and excitation forces. It has also been validated with experiments, semi-analytical solutions and cross-model validation for a number of different structural geometries used within the field of renewables ([2], [17]). It has OpenMP parallelization implemented which allows it to be at par or even faster than WAMIT for some deep water cases.

The current study further develops the capabilities of HAMS-MREL with the validation of new features. These features include the calculation of individual fields for diffraction and radiation for free surface elevation and pressure, global plane of symmetry, suppression of irregular frequencies and generalized modes. HAMS-MREL v1.0 is the currently available open-source version of HAMS-MREL. The parallelization with OpenMP has already been applied to the calculation of the Green's function, the solution of the set of linear algebraic equations to obtain the potentials and the calculation across a number of incident wave directions. In HAMS-MREL v2.0, these new features will be implemented with OpenMP parallelization, thus immensely improving their computational gain .

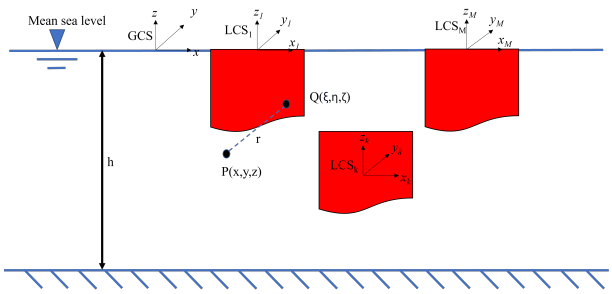

Fig. 1: Definition of the coordinate system for the multiple body interaction problem. GCS refers to the global coordinate system and LCS refers to the local coordinate system per body. Q denotes the source point on the immersed body surface and P denotes the field point anywhere in the fluid domain. (This figure is taken from [17])

II. Current framework of HAMS-MREL

HAMS-MREL solves the diffraction and radiation multiple body problem, based on the linear potential flow theory considering relevant boundary conditions. The flow is described through a total complex-valued spatial velocity potential $\phi(\mathbf{x})$ for all considered bodies which can be expressed as the summation of three parts: the complex-valued spatial incident wave potential $\phi_I(\mathbf{x})$, the complex-valued spatial scattered potential $\phi_S(\mathbf{x})$ and the complex-valued spatial radiated potential $\phi_R(\mathbf{x})$. Here, $\mathbf{x}$ refers to the cartesian coordinates (x, y, z) expressed in m. This is shown as:

$$\phi(\mathbf{x}) = \phi_I(\mathbf{x}) + \phi_S(\mathbf{x}) + \phi_R(\mathbf{x}) = \phi_D(\mathbf{x}) + \phi_R(\mathbf{x}) \quad (1)$$

where ϕ_D is the complex-valued diffraction potential.

The potential satisfies the Laplace equation.

$$\nabla^2\phi = 0 \quad (2)$$

When considering the diffraction and radiation problem, the following boundary conditions are considered.

- The free surface boundary condition

$$\frac{\partial\phi_l}{\partial z} = \mu\phi_l, z = 0 \quad (3)$$

- The body boundary condition

$$\frac{\partial\phi_D}{\partial n} = 0, \frac{\partial\phi_j^{(k)}}{\partial n} = n_j^{(k)}, \text{on } S_B^{(k)} \quad (4)$$

  where $S_B^{(k)}$ is the body surface of the k^{th} body.
- The sea bottom boundary condition

$$\frac{\partial\phi_l}{\partial z} = 0, z = -h, \text{or } z \to \infty \quad (5)$$

- Sommerfield's radiation condition

$$\lim_{R\to\infty}[\sqrt{\mu R}(\frac{\partial\phi_l}{\partial R} - i\mu\phi_l)] = 0 \quad (6)$$

$\mu = \omega^2/g$ is the deepwater wave number and g is the acceleration due to gravity. h denotes the water depth considering finite depth, R is the horizontal distance from any of the bodies and $'i'$ refers to the imaginary unit with its coefficient referring to the imaginary part of a complex number. $\phi_j^{(k)}$ refers to the radiation potential of the fluid velocity field generated by the j^{th} degree of freedom (dof) for the k^{th} body. j = 1,...,6 and k = 1,...,M. $n_j^{(k)}$ is the normal vector in the j^{th} dof for the k^{th} body. ϕ_l can be ϕ_D or $\phi_j^{(k)}$ depending on if it is diffraction or radiation.

The total velocity potential in HAMS-MREL can then be defined as follows.

$$\phi(\mathbf{x}) = \phi_D(\mathbf{x}) - i\omega\sum_{j=1}^{6M}\zeta_j\phi_j(\mathbf{x}) \quad (7)$$

where ζ_j represent the complex motion amplitudes in each mode.

The boundary integral equation for the diffraction problem (for the complex-valued scatter potential) considering these boundary conditions with $S_B^T = S_B^{(1)} + S_B^{(2)} + ... + S_B^{(M)}$ is given as follows.

$$2\pi\phi_S(\mathbf{x}) + \iint_{S_B^T}\phi_S(\xi)\left(\frac{\partial G(\xi;\mathbf{x})}{\partial n_\xi}\right)dS_\xi = -\iint_{S_B^T}\left(\frac{\partial\phi_I}{\partial n}\right)G(\xi;\mathbf{x})dS_\xi \quad (8)$$

Here $\mathbf{x}$ refers to the field point, ξ refers to the source point, G is the Green's function and the subscript $'I'$ indicating the incident wave. Similar to the diffraction problem, the boundary integral equation for the complete radiation problem can be given as follows.

$$2\pi\phi_j^{(k)}(\mathbf{x}) + \iint_{S_B^T}\phi_j^{(k)}(\xi)\left(\frac{\partial G(\xi;\mathbf{x})}{\partial n_\xi}\right)dS_\xi = \iint_{S_B^{(k)}}G(\xi;\mathbf{x})n_j^{(k)}dS_\xi \quad (9)$$

By utilizing the 'collection' method wherein the centroids of the panels represent the collection points, the boundary integral equation for the diffraction problem and radiation problem are solved to obtain the potentials [17].

Once the velocity potentials on the body surfaces are obtained, the hydrodynamic coefficients and excitation forces can be computed. By integrating the pressure multiplied by the j^{th} component of the normal vector over the k^{th} body, the hydrodynamic forces acting in the j^{th} dof of the k^{th} body can be computed. These are as follows.

$$E_j^{(k)} = i\omega\rho\iint_{S_B^k}\phi_D n_j^{(k)}dS \quad (10)$$

$$A_{js}^{(k)(q)} + (i/\omega)B_{js}^{(k)(q)} = \rho\iint_{S_B^k}\phi_j^{(q)}n_s^{(k)}dS \quad (11)$$

where $E_j^{(k)}$ is the wave excitation force in the j^{th} dof of the k^{th} body, and $A_{js}^{(k)(q)}$ and $B_{js}^{(k)(q)}$ are the added mass and radiation damping coefficients, respectively, in the s^{th} dof of the k^{th} body due to the j^{th} mode of motion of the q^{th} body.

The new features showcased in the next section are built upon this current framework in HAMS-MREL.

III. New features in HAMS-MREL

This section focuses on the validation of the new features in HAMS-MREL. For all the new features, the simulations were performed in Snellius High Performance Computer (SURF Netherlands) in a 64 GB node with AMD Rome 7H12 processor (3.3 GHz).

A. Wave fields

The wave fields comprise of the pressure and free-surface elevation fields. HAMS-MREL is capable of calculating both these quantities. However, for the purposes of this study, only the free-surface elevation is showcased.

The free-surface elevation $\eta(\mathbf{x}, t)$ can be obtained from the total velocity potential. This is obtained from the dynamic free-surface condition as follows.

$$\eta(\mathbf{x}, t) = -\frac{1}{g}\left(\frac{\partial \phi(\mathbf{x}, t)}{\partial t}\right)_{z=0} \tag{12}$$

In the frequency domain, the complex-valued free surface elevation $\eta(\mathbf{x})$ is given below.

$$\eta(\mathbf{x}) = \frac{i\omega}{g}\phi(\mathbf{x})_{z=0} \tag{13}$$

To validate the free-surface elevation wavefield in HAMS-MREL, a simulation of a three cylinder case was run and compared with WAMIT. The free-surface elevation for diffraction and radiation are individually considered here. The case is taken from the work of Raghavan et.al. [17]. The case is shown in Fig. 2 and the mesh is shown in 3. The properties of the case are shown in Table I.

Fig 4 and Fig 5 show the non-dimensional diffraction free-surface elevation η_D/A and non-dimensional radiation free-surface elevation $\eta_3^{(2)}/A$. The obtained fields compare very well with WAMIT giving a Mean Squared Error (MSE) of less than 1 %.

TABLE I: Properties of the three cylinder case for obtaining wave fields

Property	Value
Diameter, D (m)	6
Draft, d (m)	10.95
Water depth, h (m)	120
Spacing, L (m)	15
Incident wave angle, β (deg)	0
Amplitude of wave, A (m)	1

B. Global symmetry

The computational efficiency of the solution from HAMS-MREL can be significantly improved by utilizing symmetry. With the current implementation, a single global plane of symmetry (either along x or y) can be utilized ([18], [25]). The discretized form of the boundary integral equation (diffraction or radiation) can be expressed as follows.

$$[A]\{\phi\} = \{B\} \tag{14}$$

Considering a single plane of symmetry, it is possible to partition the matrix A, vector ϕ and matrix B (see Fig. 6, where the partition is made about y=0. This indicates that for the panels in +y, the vector with the potential is given as ϕ_2. For the panels in -y, the vector with the potential is given as ϕ_1).

In order to reduce the number of linear equations to be solved, an orthogonal transformation matrix $[R]$ can be utilized such that

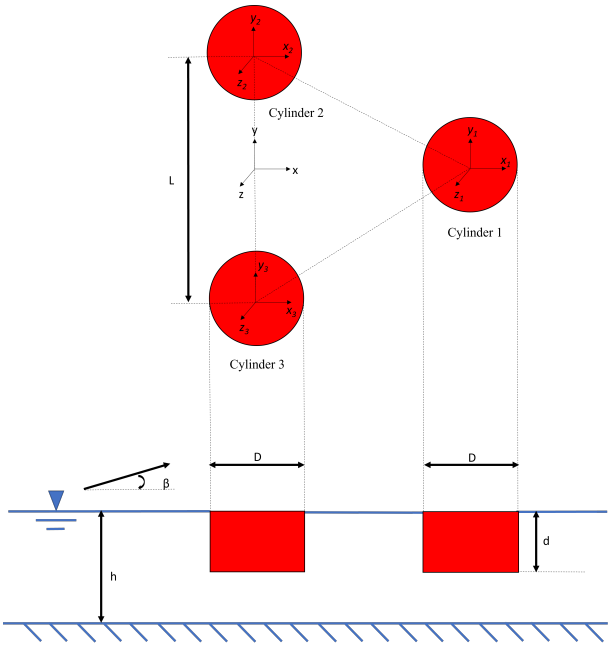

Fig. 2: Three cylinder case - wave fields (This figure is taken from [17])

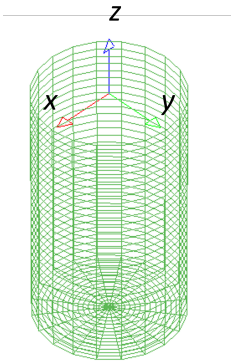

Fig. 3: Cylindrical mesh with 900 panels used for computing wave fields

$$[\widehat{A}] = \frac{1}{\gamma}[R][P][R] \tag{15}$$

$$\{\widehat{\phi}\} = [R]\{\phi\} \tag{16}$$

$$\{\widehat{B}\} = [R]\{B\} \tag{17}$$

with γ = 2, since there are two regions due to a single plane of symmetry. The transformation reduces the linear system to a simplified diagonal form

$$\begin{bmatrix} \widehat{A}^{(1)} & 0 \\ 0 & \widehat{A}^{(2)} \end{bmatrix} \begin{bmatrix} \widehat{\phi}^{(1)} \\ \widehat{\phi}^{(2)} \end{bmatrix} = \begin{bmatrix} \widehat{B}^{(1)} \\ \widehat{B}^{(2)} \end{bmatrix} \tag{18}$$

From this $\{\widehat{\phi}\}$ can be obtained.

In order to demonstrate the application of symmetry, a single row of floating cylinders is considered. This is shown in Fig. 7, where three cylinders are considered. The mesh for one of the cylinders is shown in Fig. 8a. The properties for the case are given in Table II. The half cylinder mesh utilized thanks to the symmetry is shown in Fig. 8b.

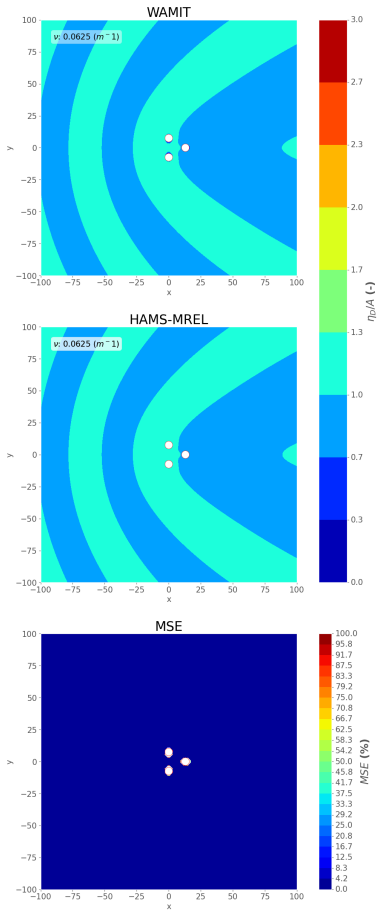

Fig. 4: Non-dimensional diffraction wave field η_D/A for wavenumber ν = 0.0625 m^{-1} and νh = 7.5 (deep waters)

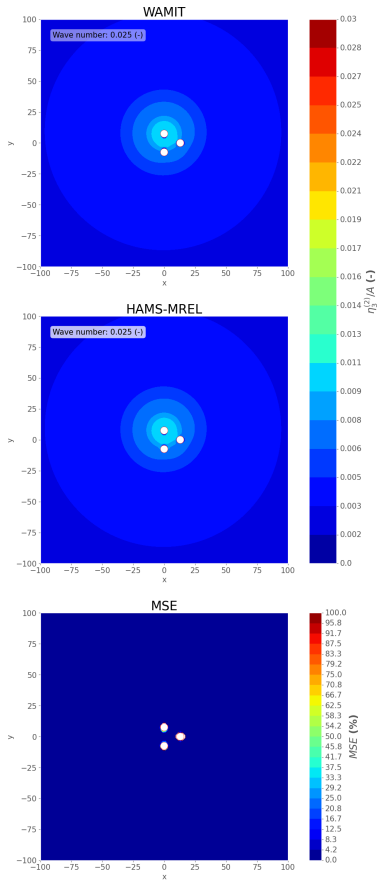

Fig. 5: Non-dimensional radiation wave field $\eta_3^{(2)}/A$ for wavenumber ν = 0.025 m^{-1} and νh = 3 (deep waters)

TABLE II: Properties of the Three cylinder case for symmetry

Property	Value
Diameter, D (m)	6
Draft, d (m)	1.5
Water depth, h (m)	120
Spacing, L (m)	18
Incident wave angle, β (deg)	0
Number of frequencies, N_ω (-)	300

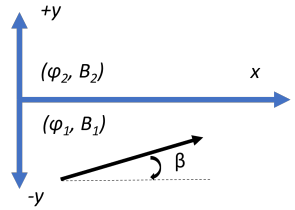

Fig. 6: Symmetry partitioning - symmetry plane y=0

Two cases, one with symmetry and another without symmetry are considered. As seen from Fig. 9, for both cases, the results of the hydrodynamic coefficients and excitation forces match perfectly. A spike is observed close to the wave period of 2 s resulting from an irregular frequency. Its suppression will be demonstrated in the next section.

When comparing the computational gain due to the application of symmetry, without considering parallelization, a factor of 3.0 was obtained, which would be beneficial when analysing large arrays.

C. Suppression of irregular frequencies

When solving the BIEs in HAMS-MREL, substantial errors can occur at 'irregular frequencies'. This is observed as a significant jump or dip in the hydrodynamic coefficients and excitation forces, and can result in unrealistic estimations of the response of floating structures.

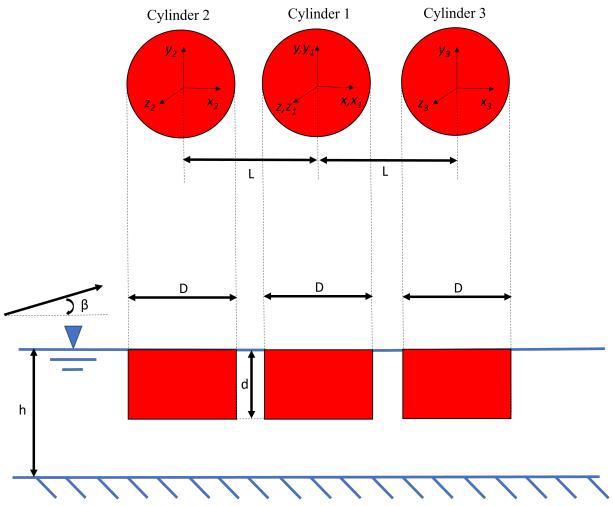

Fig. 7: Three cylinder case

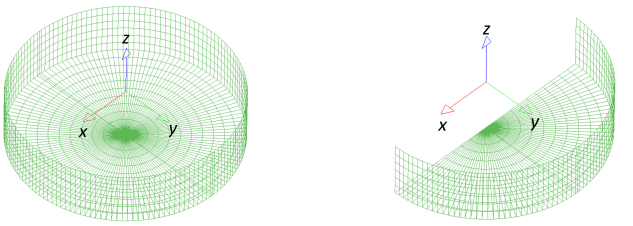

(a) Whole cylinder mesh (b) Half cylinder mesh

Fig. 8: Cylinder mesh and half cylinder mesh - Symmetry

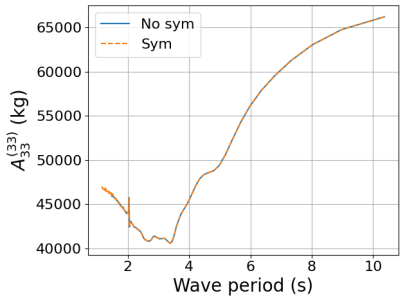

(a) Heave added mass

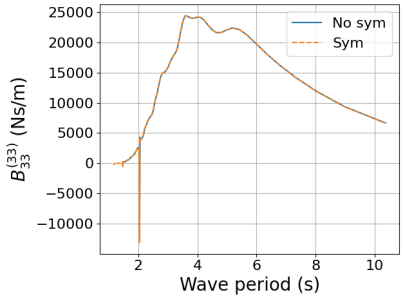

(b) Heave radiation damping

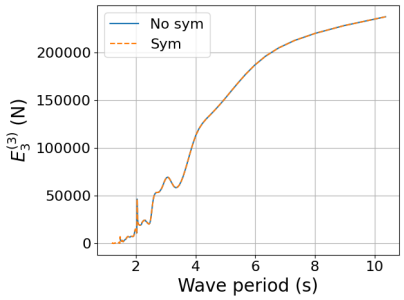

(c) Heave excitation force

Fig. 9: Hydrodynamic coefficients and excitation forces for heave for Cylinder 1 - Symmetry

Irregular frequencies are purely numerical and arise from ill-conditioning of the boundary integral problems [26]. These coincide with the eigen frequencies of the hypothetical sloshing modes (flow that fills the interior of the structure), which are obtained from the internal Dirichlet problem [27] and are numerically caused by the interaction of the water-plane section of floating bodies intersecting with the free-water surface [28].

An extended BIE is thus developed and utilized, which assumes the potentials on the interior of the water plane are zero. This is only performed for bodies where the input waterplane mesh is provided (In HAMS-MREL, it is possible to provide the water plane mesh for specific bodies). By applying the Green's equation in the interior of the floating body, additional BIEs are introduced which are combined with the conventional BIEs.

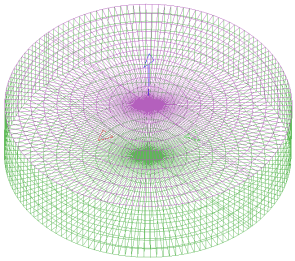

Fig. 10: Water plane mesh (pink) together with the cylinder mesh (green)

Considering the total number of elements as N_{WP}^T for all the water plane meshes and N_P^T for all the considered bodies, a set of overdetermined linear algebraic equations are obtained by combining the additional BIE on the waterplane with the conventional BIE.

$$[A]_{(N_{WP}^T+N_P^T)XN_P^T}\{\phi\}_{N_P^T} = [B]_{(N_{WP}^T+N_P^T)XN_P^T} \tag{19}$$

The least squares method implemented for solving the set of linear algebraic equations implemented in HAMS, is extended to this problem. For more details, see [28].

In order to validate the suppression of irregular frequencies with HAMS-MREL, the three cylinder case from the previous section (see Fig. 7) is utilized. It was observed from Fig. 9, that a spike was observed close to 2 s. The waterplane mesh is shown in Fig. 10 .To make a comparison with and without the suppression of irregular frequencies, three different simulations were preformed

- Simulation 1 - No suppression of irregular frequencies (No-IR)
- Simulation 2 - Suppression of irregular frequencies for Cylinder 1 and 2 (IR-2)
- Simulation 3 - Suppression of irregular frequencies for all cylinders (IR-all)

The results are shown in Fig. 11. When considering the three cylinder case with no irregular frequency suppression, it is observed that the irregular frequency occurs at around 2 s for all the cylinders. This can be seen in the 'No-IR' simulation in Fig. 11 (a)-(c). When considering Simulation 2, wherein the waterplanes are only utilized for Cylinder 1 and 2, it is observed that the irregular frequency is suppressed while it is not suppressed for Cylinder 3. When the waterplane mesh is used in all cylinders, the irregular frequency for each cylinder is suppressed for all cylinders.

D. Generalized modes (Dry modes) approach

The generalized modes approach can be used to model flexible structures or structures with constraints,

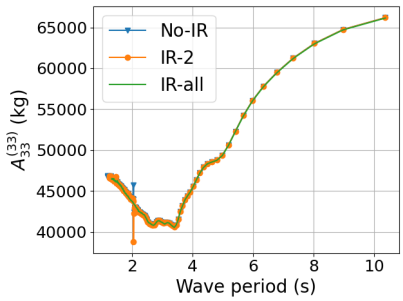

(a) Cyl 3 - Heave added mass

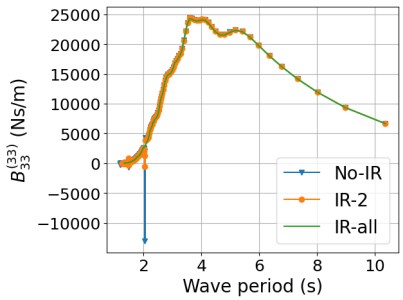

(b) Cyl 3 - Heave radiation damping

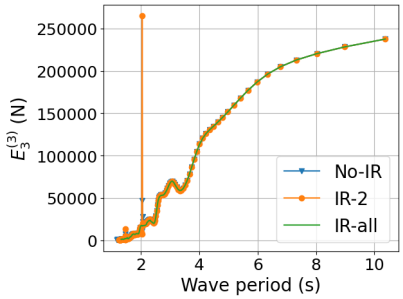

(c) Cyl 3 - Heave excitation force

Fig. 11: Hydrodynamic coefficients and excitation forces for heave for Cylinder 3

an example of such bodies are attenuator/terminators wave energy converters, and/or large floating bodies with several hinged components. In order to incorporate any generic motion of the structure, the body boundary condition in the BIEM problem needs to be modified. This is based on the dry modes approach introduced in [29].

The body boundary condition (Eqn 4) can be expressed as a general expression:

$$\frac{\partial \phi_j^{(k)}}{\partial n} = \mathbf{S_j^{(k)}}.\mathbf{n^{(k)}} \tag{20}$$

where $\mathbf{S_j^{(k)}}$ is a 3D vector shape function of the k^{th} body, with cartesian components $u_j^{(k)}, v_j^{(k)}, w_j^{(k)}$ and $\mathbf{n^{(k)}} = (n_x^{(k)}, n_y^{(k)}, n_z^{(k)})$ is the normal vector projecting from the k^{th} body towards the fluid [29]. In general, for the rigid body translational degrees of freedom (j = 1,2,3), the shape function is a unit vector in the corresponding direction, and for the rigid body rotations (j=4,5,6), $\mathbf{S_j} = \mathbf{S_{j-3}} \times \mathbf{r}$, where $\mathbf{r}$ is the lever arm vector with respect to a rotation center([29], [30]).

The projection of the normal vector can then be written as follows.

$$\mathbf{S_j^{(k)}}.\mathbf{n^{(k)}} = u_j^{(k)} n_x^{(k)} + v_j^{(k)} n_j^{(k)} + w_j^{(k)} n_z^{(k)} \tag{21}$$

TABLE III: Properties of the flap(all dimensions in m)

Part	Dimension ($W \times T \times H$)
Flap top	
Rectangular box	18 × 1.8 × 8.5
Triangular box	18 × 0 - 1.8 × 0.9
Flap bottom	
Rectangular box	18 × 1.8 × 1.5

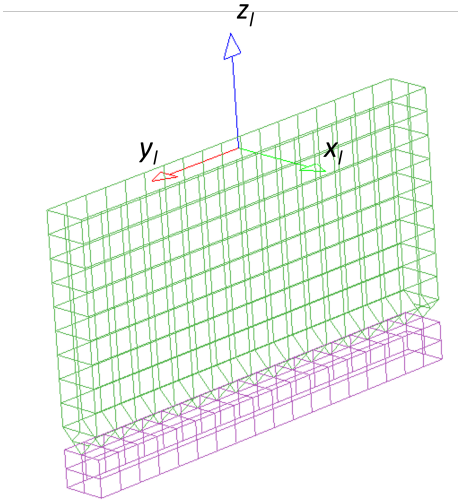

Fig. 12: Mesh of the flap in HAMS-MREL - top (green) and bottom (pink) - from [22]

Therefore, by deriving this vector shape function for any additional mode/degree of freedom, the radiation and diffraction problem can also be solved considering this degree of freedom in HAMS-MREL.

In order to demonstrate this approach in HAMS-MREL, the rigid flap from the work of Van 'T Hoff [31] is taken, which has been validated with scaled experiments. The derivation of the shape function has been done in Raghavan et.al. [22]. Therefore, the shape function is summarized here.

The flap is modelled as a two body problem, where the top and bottom are two different bodies. The geometry of the flap is shown in Fig 13. The flap top combines two geometries, a rectangular box and a triangular box, while the flap bottom, which is rigidly fixed to the sea bottom, is composed of a rectangular box. The dimensions of these parts is shown in Table III. The hinge is located at L_s = 8.9 m from the free surface. The water depth is 10.9 m, thus the hinge being at 2 m above the sea bottom.

The shape function for the additional degree of freedom/mode shape for the flap top is given as follows.

$$\mathbf{S_7^{(1)}} = (L_s + z, 0, -x) \tag{22}$$

Since the flap bottom is stationary, the shape function for the bottom is a null vector.

$$\mathbf{S_7^{(2)}} = (0, 0, 0) \tag{23}$$

Using this as the body boundary condition for the additional pitch motion about the hinge, the radiation and diffraction problems can be solved to obtain the hydrodynamic coefficients and excitation forces.

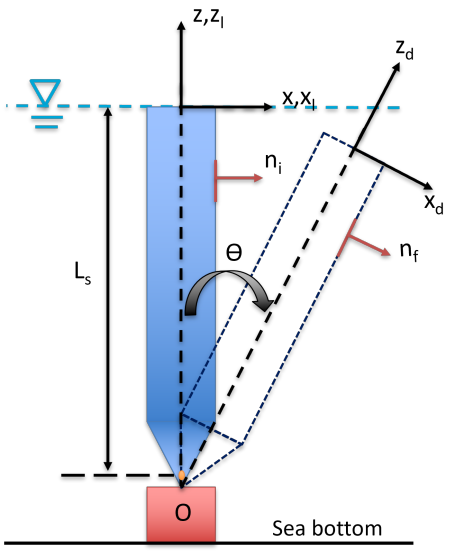

Fig. 13: Schematic representation of rotation of the flap (from [22])

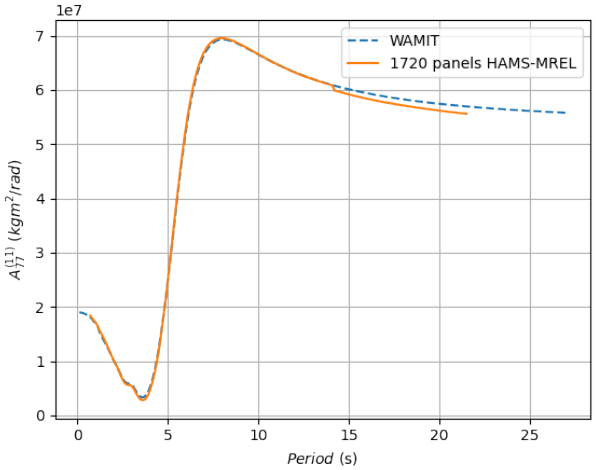

Fig. 14: Added mass flap $A_{77}^{(11)}$

The cross-model validation with the commercial solver WAMIT was performed. The considered geometry and results for the hydrodynamic coefficients and excitation force for the flap, were taken from the work of Van 'T Hoff [31], since this was experimentally validated. However, it should be noted that Van 'T Hoff utilized a slightly lower resolution mesh as compared to the converged mesh resolution with WAMIT, since the influence on the final results was little.

A convergence study was performed for choosing the number of panels. With 1720 panels, good convergence is achieved. Considering the added mass, $A_{77}^{(11)}$ (see 14), it is observed that the two solvers match very well till 14 s. Beyond 14 s, there is a small underestimation from HAMS-MREL, which is less than 5%. It is stated here again, that the mesh utilized in WAMIT has a mesh resolution lower than the converged mesh. Hence it is expected, that smaller differences would be observed when using a higher resolution mesh.

When considering the radiation damping coefficient (given as $B_{77}^{(11)}$), both the solvers are generally close

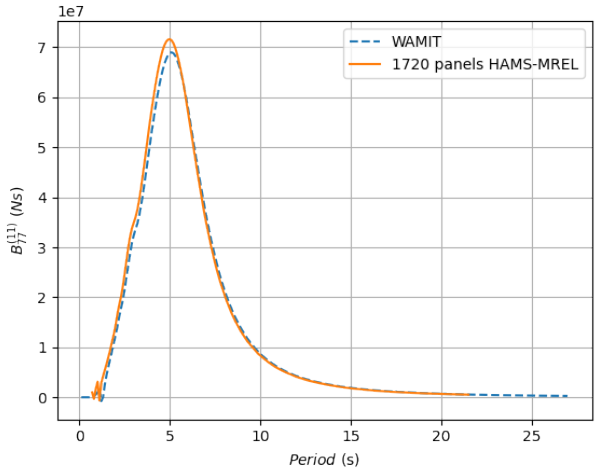

Fig. 15: Radiation damping flap $B_{77}^{(11)}$

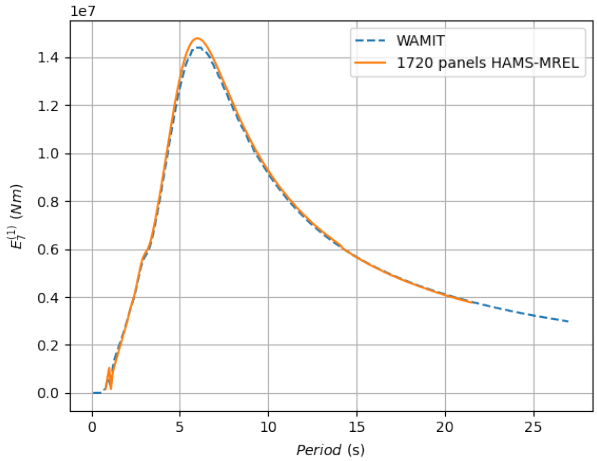

Fig. 16: Excitation force flap $E_7^{(1)}$

with HAMS-MREL slightly overestimating close to the peak at 5 s.

The results for the excitation forces $E_7^{(1)}$ are shown in Fig 16. When considering the excitation forces, both solvers are close, with slight overestimation (of about 5%) close to the peak at 6 s.

The slight overestimation with the peaks of $B_{77}^{(11)}$ and $E_7^{(1)}$, and the slight difference in the location of the peaks between WAMIT and HAMS-MREL with regard to $B_{77}^{(11)}$, could also be due to the mesh utilized in WAMIT having mesh resolution lower than the converged mesh.

An unusual peak is observed at the low period of 1 s in both the radiation damping coefficient and excitation force, and is less pronounced in the added mass coefficient. This can be attributed to the irregular frequency, which is usually observed at high wave frequencies. This can be nullified by using a waterplane mesh in addition to the hull mesh, and solving the extended boundary value problem (refer Section III-C). This is however, not relevant for this section.

IV. Conclusions

The paper presents the validation of the new features in open-source BIEM solver HAMS-MREL. These

includes free-surface elevation and pressure fields (together referred to as wave fields), global symmetry, suppression of irregular frequencies and generalized modes (dry modes) approach.

When considering the wave fields, the case of the three cylinder array in a triangular configuration is considered and the free-surface diffraction and radiation fields are obtained. Cross-model validation is performed for the RAOs and wave fields with the commercial solver WAMIT. Both the diffraction and radiation free surface elevation fields are seen to match very well between the two solvers with less than 3% error.

When considering the implementation of the global symmetry, the case of a single line of three cylinders is considered. The hydrodynamic coefficients and excitation forces were the same with and without symmetry which validates this feature. A gain by a factor of 3.0 was obtained in this case.

When considering the suppression of irregular frequencies, the same case of three cylinders as used for global symmetry is considered. It is observed that HAMS-MREL is able to suppress the irregular frequencies based on the utilization of the water plane mesh for solving the extended BIEM problem.

When considering the generalized modes approach, the case of a two body flap is considered, where the flap bottom is stationary. The implemented shape function is taken from our previous work [22], and validated with WAMIT. With a mesh resolution of 1720 panels, results between the solvers are close (less than 3%).

With the aforementioned features, the open-source solver HAMS-MREL has been significantly enhanced. With this research, the authors hope to contribute to the open-source domain; and enable the development of highly accurate and highly efficient numerical tools, for the deployment of marine renewable energy arrays.

V. Future work

A journal paper is currently under review with the theory and validation of these new features in HAMS-MREL. This work also provides a detailed analysis of these features and examines the parallelization techniques implemented in HAMS-MREL, which have been extended to enhance them.

The features introduced in this paper are part of the HAMS-MREL v2.0. The code will be made available on Gitlab as well as the MREL website (under the tab Datasets & Models) - www.tudelft.nl/ceg/mrel.

Acknowledgement

The authors would like to thank Yingyi Liu, the creator of HAMS for the initial discussions regarding the original code. Without his original robust code, this implementation would not have been possible. The authors would like to thank Jos Van 'T Hoff for sharing his results, as part of his PhD dissertation, which have been utilized for validation. The authors would also like to thank and acknowledge the discussions with Georgia Sismani, Eva Loukogeogaki, Nikos Mantadakis and Matthieu Ancellin.

The authors would also like to acknowledge SURF and access to the HPC Snellius for running the simulations in HAMS-MREL, under project EINF3290.

References

[1] M. Alves, "Chapter 2 - frequency-domain models," in *Numerical Modelling of Wave Energy Converters*, M. Folley, Ed. Academic Press, 2016, pp. 11–30. [Online]. Available: https://www.sciencedirect.com/science/article/pii/B9780128032107000025

[2] V. Raghavan, I. Simonetti, A. V. Metrikine, G. Lavidas, and L. Cappietti, "A new numerical modelling framework for fixed oscillating water column wave energy conversion device combining bem and cfd methods: Validation with experiments," *Ocean Engineering*, vol. 301, p. 117543, 2024. [Online]. Available: https://www.sciencedirect.com/science/article/pii/S0029801824008801

[3] C.-H. Lee and J. N. Newman, "Computation of wave effects using the panel method," 2003. [Online]. Available: https://api.semanticscholar.org/CorpusID:17331425

[4] D. G. Software, *WADAM - SESAM User Manual*, DNV GL, 2018.

[5] B. Veritas, "Hydrostar Hydrodynamic Solver," https://marine-offshore.bureauveritas.com/hydrostar-software-powerful-hydrodynamic, 2024, [Online; accessed 12-December-2024].

[6] ANSYS, *ANSYS AQWA v14.5*, ANSYS, Inc., 2012.

[7] F. P. Chau and R. E. Taylor, "Second-order wave diffraction by a vertical cylinder," *Journal of Fluid Mechanics*, vol. 240, p. 571–599, 1992.

[8] *Software Framework to Accelerate BEM Linear Wave Load Program Using OpenMP (OREGEN-BEM)*, ser. International Ocean and Polar Engineering Conference, vol. All Days, 06 2023.

[9] L. Sun, P. Stansby, J. Zang, E. Moreno, and P. Taylor, "Linear diffraction analysis for optimisation of the three-float multi-mode wave energy converter m4 in regular waves including small arrays," *Journal of Ocean Engineering and Marine Energy*, vol. 2, pp. 429–438, 2016. [Online]. Available: https://link.springer.com/article/10.1007/s40722-016-0059-1#citeas

[10] H. Wolgamot, P. Taylor, and R. Eatock Taylor, "The interaction factor and directionality in wave energy arrays," *Ocean Engineering*, vol. 47, pp. 65–73, 2012. [Online]. Available: https://www.sciencedirect.com/science/article/pii/S0029801812001138

[11] H. Wolgamot, R. Eatock Taylor, and P. Taylor, "Effects of second-order hydrodynamics on the efficiency of a wave energy array," *International Journal of Marine Energy*, vol. 15, pp. 85–99, 2016, selected Papers from the European Wave and Tidal Energy Conference 2015, Nante, France. [Online]. Available: https://www.sciencedirect.com/science/article/pii/S2214166916300170

[12] *Hydrodynamic Analysis of Different Configurations of the M4 Wave Energy Converter System Using OREGEN*, ser. International Conference on Offshore Mechanics and Arctic Engineering, vol. Volume 7: Ocean Renewable Energy, 06 2024. [Online]. Available: https://doi.org/10.1115/OMAE2024-123824

[13] G. Li, P. Stansby, and S. Draycott, "General formulation for floating body with elastic mooring in irregular waves: A hybrid linear and nonlinear framework and validation," *Marine Structures*, vol. 96, p. 103623, 2024. [Online]. Available: https://www.sciencedirect.com/science/article/pii/S0951833924000510

[14] A. Babarit and G. Delhommeau, "Theoretical and numerical aspects of the open source BEM solver NEMOH," in *11th European Wave and Tidal Energy Conference (EWTEC2015)*, ser. Proceedings of the 11th European Wave and Tidal Energy Conference, Nantes, France, 2015. [Online]. Available: https://hal.science/hal-01198800

[15] R. Kurnia and G. Ducrozet, "Nemoh: Open-source boundary element solver for computation of first- and second-order hydrodynamic loads in the frequency domain," *Computer Physics Communications*, vol. 292, p. 108885, 2023. [Online]. Available: https://www.sciencedirect.com/science/article/pii/S0010465523002308

[16] M. Ancellin and F. Dias, "Capytaine: a python-based linear potential flow solver," *Journal of Open Source Software*, vol. 4, p. 1341, 2019.

[17] V. Raghavan, E. Loukogeorgaki, N. Mantadakis, A. V. Metrikine, and G. Lavidas, "HAMS-MREL, a new open source multiple body solver for marine renewable energies: Model description, application and validation," *Renewable Energy*, vol. 237, p. 121577, 2024. [Online]. Available: https://www.sciencedirect.com/science/article/pii/S0960148124016458

[18] Y. Liu, S. Yoshida, C. Hu, M. Sueyoshi, L. Sun, J. Gao, P. Cong, and G. He, "A reliable open-source package for performance evaluation of floating renewable energy systems in coastal and offshore regions," *Energy Conversion and Management*, vol. 174, pp. 516–536, 2018. [Online]. Available: https://www.sciencedirect.com/science/article/pii/S0196890418308562

[19] Y. Liu, "Introduction of the open-source boundary element method solver hams to the ocean renewable energy community," 09 2021.

[20] E. Uzunoglu, Y. Liu, and C. Guedes Soares, *Performance of the open-source potential flow solver HAMS in estimating the hydrodynamic properties of a floating wind turbine*, 10 2022, pp. 619–627.

[21] V. Raghavan, G. Lavidas, A. Metrikine, N. Mantadakis, and E. Loukogeorgaki, "A comparative study on BEM solvers for wave energy converters." CRC Press, 2022, pp. 441–447. [Online]. Available: https://www.taylorfrancis.com/books/9781003360773/chapters/10.1201/9781003360773-50

[22] V. Raghavan, A. Metrikine, G. Lavidas, T. Islam, and V. Venugopal, "Extension of hams with the generalized modes approach," in *Innovations in Renewable Energies Offshore - Proceedings of the 6th International Conference on Renewable Energies Offshore, RENEW 2024*, ser. Innovations in Renewable Energies Offshore - Proceedings of the 6th International Conference on Renewable Energies Offshore, RENEW 2024, C. Soares and S. Wang, Eds. CRC Press / Balkema - Taylor and Francis Group, 2024, pp. 193–199, 6th International Conference on Renewable Energies Offshore, RENEW 2024 ; Conference date: 19-11-2024 Through 21-11-2024.

[23] V. Raghavan, G. Lavidas, and A. V. Metrikine, "Comparing open-source bem solvers for analysing wave energy converters," *Journal of Physics: Conference Series*, vol. 2647, no. 7, p. 072002, jun 2024. [Online]. Available: https://dx.doi.org/10.1088/1742-6596/2647/7/072002

[24] W. Sheng, E. Tapoglou, X. Ma, C. Taylor, R. Dorrell, D. Parsons, and G. Aggidis, "Hydrodynamic studies of floating structures: Comparison of wave-structure interaction modelling," *Ocean Engineering*, vol. 249, p. 110878, 2022. [Online]. Available: https://www.sciencedirect.com/science/article/pii/S0029801822003183

[25] T. Matsui, K. Kato, and T. Shirai, "A hybrid integral equation method for diffraction and radiation of water waves by three-dimensional bodies," *Computational Mechanics*, vol. 2, p. 119–135, 1987. [Online]. Available: https://doi-org.tudelft.idm.oclc.org/10.1007/BF00282134

[26] T. Kelly, I. Zabala, Y. Peña-Sanchez, M. Penalba, J. V. Ringwood, J. C. Henriques, and J. M. Blanco, "A post-processing technique for removing 'irregular frequencies' and other issues in the results from bem solvers," *International Marine Energy Journal*, vol. 5, no. 1, p. 123–131, Jun. 2022. [Online]. Available: https://marineenergyjournal.org/imej/article/view/114

[27] S. Marburg and S. Amini, "Cat's eye radiation with boundary elements: Comparative study on treatment of irregular frequencies," *Journal of Computational Acoustics*, vol. 13, 03 2005.

[28] Y. Liu, "HAMS: A frequency-domain preprocessor for wave-structure interactions—theory, development, and application," *Journal of Marine Science and Engineering*, vol. 7, no. 3, 2019. [Online]. Available: https://www.mdpi.com/2077-1312/7/3/81

[29] J. Newman, "Wave effects on deformable bodies," *Applied Ocean Research*, vol. 16, no. 1, pp. 47–59, 1994. [Online]. Available: https://www.sciencedirect.com/science/article/pii/0141118794900132

[30] G. Sismani and E. Loukogeorgaki, "Frequency-based investigation of a floating wave energy converter system with multiple flaps," *Applied Mathematical Modelling*, vol. 84, pp. 522–535, 2020. [Online]. Available: https://www.sciencedirect.com/science/article/pii/S0307904X20302067

[31] J. Van 'T Hoff, "Hydrodynamic modelling of the oscillating wave surge converter," Ph.D. dissertation, Queens University Belfast, 2009.